

# MAGNETIC FIELD DECAY DUE TO THE WAVE-PARTICLE RESONANCES IN THE OUTER CRUST OF THE NEUTRON STAR

HIROYUKI R. TAKAHASHI<sup>1</sup>, KEI KOTAKE<sup>1,2</sup>, AND NOBUTOSHI YASUTAKE<sup>2</sup>

*Accepted for publication to ApJ*

## ABSTRACT

Bearing in mind the application to the outer crust of the neutron stars (NSs), we investigate the magnetic field decay by means of the fully relativistic Particle-In-Cell simulations. Numerical computations are carried out in 2-dimensions, in which the initial magnetic fields are set to be composed both of the uniform magnetic fields that model the global fields penetrating the NS and of the turbulent magnetic fields that would be originated from the Hall cascade of the large-scale turbulence. Our results show that the whistler cascade of the turbulence transports the magnetic energy preferentially in the direction perpendicular to the uniform magnetic fields. It is also found that the distribution function of electrons becomes anisotropic because electrons with lower energies are predominantly heated in the direction parallel to the uniform magnetic fields due to the Landau resonance, while electrons with higher energies are heated mainly by the cyclotron resonance that makes the distribution function isotropic for the high energy tails. Furthermore we point out that the degree of anisotropy takes maximum as a function of the initial turbulent magnetic energy. As an alternative to the conventional ohmic dissipation, we propose that the magnetic fields in the outer crust of NSs, cascading down to the electron inertial scale via the whistler turbulence, would decay predominantly by the dissipation processes through the Landau damping and the cyclotron resonance.

*Subject headings:* stars: neutron – plasmas – turbulence

## 1. INTRODUCTION

Pushed by the accumulating observations of radio pulsars, accreting neutron stars (NSs), and most recently, magnetars, extensive studies have been carried out to understand the evolution of magnetic fields in neutron stars (e.g., Bhattacharya & Srinivasan 1995; Harding & Lai 2006; Reisenegger 2009). The known radio pulsars so far are generally categorized into two classes: young ( $\lesssim 10^7$  yr) pulsars with spin periods  $P \simeq 10^{-1\sim 1}$  s and the magnetic field strength  $B \simeq 10^{10\sim 13}$  G, and the old millisecond radio pulsars, which have magnetic field strength as low as  $10^{8\sim 9}$  G. While most radio pulsars are isolated objects, the millisecond pulsars are predominantly in binaries, suggesting that the magnetic fields decay with time, perhaps by an accretion of matter from the binary companion (e.g., Harding & Lai 2006, and references therein).

For the isolated radio pulsars, it is still an open question whether the NS magnetic fields do or do not decay with time. For example, Narayan & Ostriker (1990) argued that the field should decay exponentially on a few Myr timescale (see also Cordes & Chernoff 1998; Gonthier et al. 2004), while similar studies implied the decay time  $\gtrsim 100$  Myr (e.g., Bhattacharya et al. 1992; Faucher-Giguère & Kaspi 2006). Such divergent results may come from the uncertainties inherent to those population synthesis studies, such as the selection effects, the luminosity evolution, and the dependence of beaming fraction on period. On the other hand, the discovery of magnetars has provided several important evi-

dences to favor the magnetic field decay on relatively short timescales (e.g., Arras et al. 2004; Harding & Lai 2006). In fact, the soft gamma-ray repeaters and anomalous X-ray pulsars, observed as young ( $\lesssim 10^4$  yr) NSs with strong ( $\sim 10^{14\sim 10}$  G) magnetic fields, are considered to be powered by the decay of their magnetic fields (e.g., Woods & Thompson 2006). Giant flaring activities are proposed to be the rapid release of the magnetic stress building in the NS crust (Thompson & Duncan 1995, 1996; Lyutikov 2006). More recently, Pons et al. (2007) presented an evidence that the magnetic field decay of  $\sim 10$  Myr, can explain the thermal evolution from magnetars continuously to ordinary radio pulsars. At present, these ideas and new observations seem to favor the existence of the magnetic field decay in the isolated NSs.

The pioneering study by Goldreich & Reisenegger (1992) identified the dissipation processes of the magnetic energy in the crust of the isolated NS during its evolution. They first showed that magnetized turbulence in the crust of NSs can be described by the electron magnetohydrodynamic (EMHD) equation, in which the time evolution of the magnetic field is governed by the advection of the field by the Hall drift, the Ohmic dissipation, and the ambipolar diffusion. On top of the Ohmic decay and the ambipolar diffusion, they first proposed that the Hall drift, though non-dissipative itself, could be an important ingredient for the field decay because it can lead to dissipation through the whistler cascade of the turbulence. As the eddy size of the turbulence becomes smaller, the magnetic energy was transported from large to small scales, leading to the dissipation of the magnetic energy finally via the Ohmic dissipation.

In order to confirm their prediction, numerical simulations in EMHD are required because such a cascading

takahashi@cfca.jp

<sup>1</sup> Center for Computational Astrophysics, National Astronomical Observatory of Japan, Mitaka, Tokyo 181-8588, Japan

<sup>2</sup> Division of Theoretical Astronomy, National Astronomical Observatory of Japan, Mitaka, Tokyo 181-8588, Japan

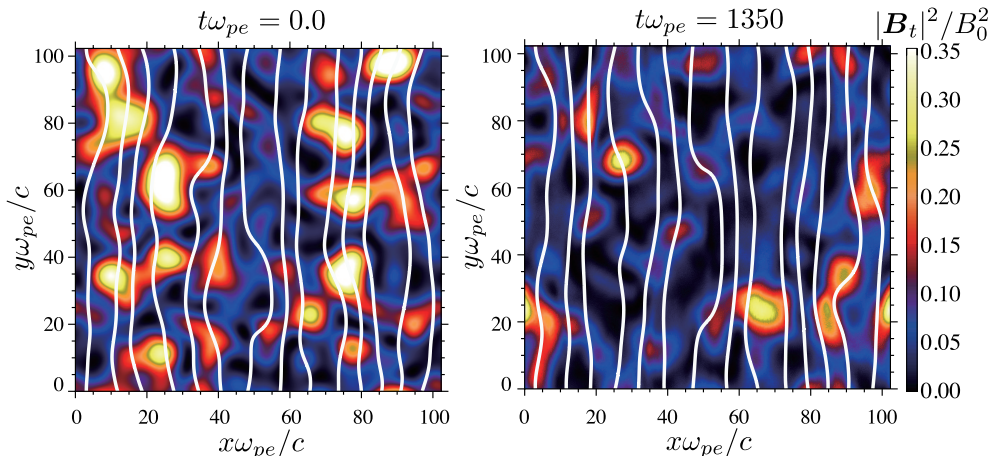


FIG. 1.— Turbulent magnetic field energy density  $|\mathbf{B}_t/B_0|^2 = |(\mathbf{B} - B_0\mathbf{e}_y)/B_0|^2$  (color) and the magnetic field lines (curves) at the initial state (left) and at  $t\omega_{pe} = 1350$  (right) for  $\epsilon = 0.1$ .

process is essentially a non-linear process. In the two- and three-dimensional (2D and 3D) simulations of the low  $\beta$  plasma, Biskamp et al. (1999) showed a clear cascade of the energy due to the whistler turbulence over more than an order of magnitude in the length scale. The 3D EMHD simulations by Cho & Lazarian (2004, 2009) confirmed the scale-dependent anisotropy in the EMHD turbulence. They also showed that the anisotropic cascading processes in the EMHD proceed via the propagation of the whistler waves along the global magnetic fields (see, also Narita & Gary 2010). This nature is in contrast to the conventional MHD turbulence, in which the Alfvén waves play a major role to transport the turbulent magnetic energy (e.g., Goldreich & Sridhar 1995; Biskamp & Welter 1989; Cho et al. 2002). Reflecting the fact that the propagation of the whistler waves are more dispersive than the Alfvén waves, the power spectral density in the EMHD turbulence was shown to become steeper compared to the MHD turbulence. Here it should be noted in the EMHD simulations that one can precisely follow the cascading process, however the dissipation process should be treated phenomenologically, i.e., via the resistivity or the so-called hyperdiffusivity (Cho & Lazarian 2004, 2009).

In this paper, we perform the Particle-In-Cell (PIC) simulations aiming to understand the decay process of the magnetic fields in NSs. As well known, the PIC simulations, which have been often performed to study the turbulent cascade in solar wind (Saito et al. 2008; Gary et al. 2008, 2010), can precisely take into account the electromagnetic modes in plasma by solving the full Maxwell equations coupling with the all species of plasma particles. The ordinary PIC simulation can treat the collisionless plasma in which the collisional frequency is smaller than the typical frequencies of plasma particles, such as the plasma frequency and the gyro frequency. Shternin & Yakovlev (2006) have estimated the collisional frequency between the particles in NSs. From their results, the electron collisional frequency in the outer crust of the NS is of the order of  $10^{-2}\omega_{pe}$  with  $\omega_{pe}$  being the electron plasma frequency, which indicates that the electrons are marginally collisionless in the electron inertial scale. Since the gyro frequency is of the order of the plasma frequency, we approximately treat

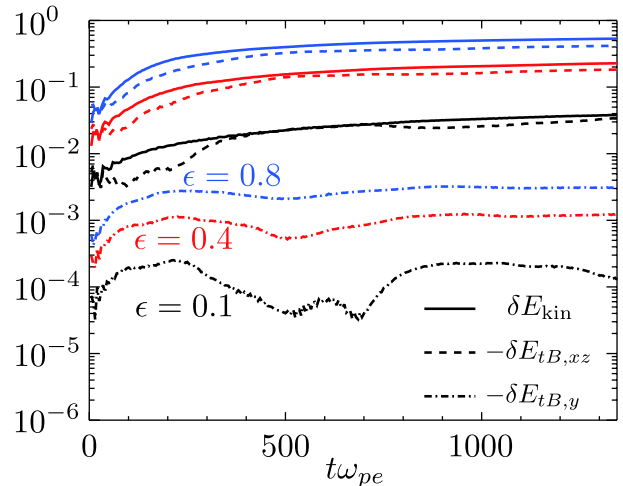


FIG. 2.— Time evolution of the energy deviation. Blue, red, black curves are respectively for  $\epsilon = 0.8, 0.4, 0.1$  and the solid, dashed, dot-dashed curves denote the electron kinetic energy ( $\delta E_{\text{kin}}$ ), the minus of the turbulent magnetic field energy whose field component is perpendicular to  $\mathbf{B}_0$  ( $-\delta E_{tB,xz}$ ), and the minus of the turbulent magnetic field energy whose field component is parallel to  $\mathbf{B}_0$  ( $-\delta E_{tB,y}$ ), respectively.

the plasma as collisionless to study the decay process of the magnetic fields in the outer crust of the NS. As a complement to the foregoing EMHD simulations (e.g., Biskamp et al. 1999; Cho & Lazarian 2004, 2009) that focus on the whistler cascade of the turbulence, the PIC simulations that we will present in this paper, should merit for understanding the mechanism of the magnetic field decay, cascading further down to the electron inertial scale.

This paper is organized as follows. In Section 2, we show the numerical setup of the PIC simulations. The numerical results of the turbulent cascade and the dissipation process are shown in § 3. We summarize our results and discuss their implications in Section 4.

## 2. NUMERICAL METHODS AND INITIAL CONDITIONS

We carry out 2-dimensional fully relativistic PIC simulations (e.g., Birdsall & Langdon 2001). The basic equations are described as,

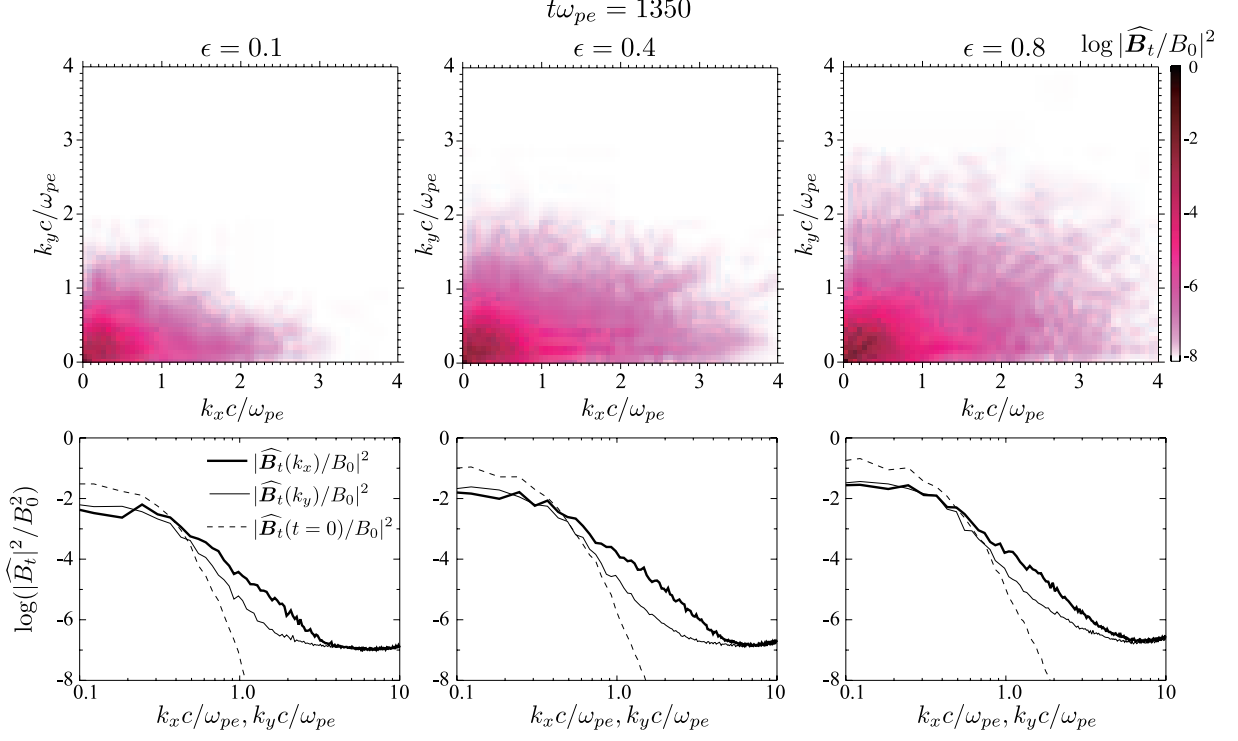


FIG. 3.— (Upper panel) Power spectral density of the turbulent magnetic fields,  $\log|\widehat{\mathbf{B}}_t/B_0|^2$  at  $t\omega_{pe} = 1350$  for  $\epsilon = 0.1, 0.4, 0.8$  from left to right, respectively. The lower panels show the 1-dimensional, cumulative power spectral density. Thick and thin solid curves show  $|\widehat{\mathbf{B}}_t(k_x)/B_0|^2$  and  $|\widehat{\mathbf{B}}_t(k_y)/B_0|^2$ , respectively, while dashed curves do the initial spectra of the turbulent magnetic energy.

$$\frac{d\mathbf{p}_i}{dt} = q_i (\mathbf{E} + \boldsymbol{\beta}_i \times \mathbf{B}) \quad (1)$$

$$\nabla \cdot \mathbf{B} = 0, \quad (2)$$

$$\nabla \cdot \mathbf{E} = 4\pi\rho_e, \quad (3)$$

$$\frac{\partial \mathbf{B}}{\partial t} + c\nabla \times \mathbf{E} = 0, \quad (4)$$

$$\frac{\partial \mathbf{E}}{\partial t} - c\nabla \times \mathbf{B} = -4\pi\mathbf{j}, \quad (5)$$

$$\rho_e = \sum_i q_i S(\mathbf{x} - \mathbf{x}_i), \quad (6)$$

$$\mathbf{j} = \sum_i q_i \mathbf{v}_i S(\mathbf{x} - \mathbf{x}_i), \quad (7)$$

where  $\mathbf{p}_i$ ,  $q_i$ ,  $\mathbf{E}$ ,  $\mathbf{B}$ ,  $\rho_e$ , and  $\mathbf{j}$  are the momentum, the particle charge, the electric fields, the magnetic fields, the charge density, and the current density, respectively.  $\boldsymbol{\beta}_i \equiv \mathbf{v}_i/c$  is the three velocity normalized by the speed of light. The subscript  $i$  denotes the particle species. Here we ignore the quantum effects such as the Landau level, for simplicity. The particle motion is determined by solving the special relativistic equation of motion. Then the electric charge and the charge current are obtained from equations (6) and (7), in which the shape factor  $S$  can extrapolate the physical quantities on discretized grids at  $\mathbf{x}$  from particles. By using the electric charge and the current density, the electromagnetic fields are updated by solving Maxwell equations, so that the system can be solved self-consistently. We solve these equations in the rectangular coordinates by assuming  $\partial/(\partial z) = 0$

(the so-called 2.5-dimension). Number of grid points is  $(N_x, N_y) = (1024, 1024)$  and the corresponding system size is  $L_x = L_y = 102.4c/\omega_{pe}$ , where  $\omega_{pe} \equiv \sqrt{4\pi n e^2/m_e}$  is the electron plasma frequency. Each cell contains 80 particles and the total number of particles in the simulation box is  $8.4 \times 10^7$  for each species. The boundary conditions are periodic in both directions. We assume that ions are immovable, which is reasonable in the outer crust of the NS (e.g., Goldreich & Reisenegger 1992). We confirmed that the numerical results are qualitatively and quantitatively consistent with those when we take into account the ion motion.

In the initial state, the plasma distributes uniformly in space and the electron distribution function obeys the relativistic Maxwellian with the temperature  $T_e = 10^8$  K (e.g., Aguilera et al. 2008). We assume that there are two components of the magnetic fields in the NS. The first one is the uniform magnetic fields that would globally penetrate the NS, which should be necessary to explain the spin-down of the NS. The global field is set to be uniform in space  $\mathbf{B} = B_0 \mathbf{e}_y$ , where  $\mathbf{e}_y$  is the unit vector in  $y$ -direction. The corresponding ratio of the gyro frequency evaluated from the uniform magnetic fields  $\omega_{ce} = eB_0/(m_e c)$  and the plasma frequency  $\omega_{pe}$  is 0.5. The second one is the turbulent magnetic fields, which would be cascaded down from large to small scales due to the Hall turbulence. The initial turbulent magnetic fields are modeled to take the form of  $\widehat{\mathbf{B}}(\mathbf{k}) \propto \exp[-\mathbf{k}^2/k_0^2 + i\alpha_k]$ , where  $\mathbf{k}$  is the wave number,  $k_0 = 0.31\omega_{pe}/c$  is the typical wave number of the initial fluctuations and  $\alpha_k$  is the random phase. The hat denotes the variable in the Fourier space. We change the amplitude of the turbulent

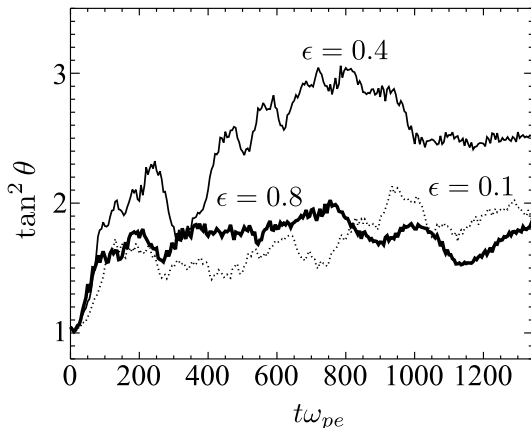


FIG. 4.— Time evolution of the anisotropy  $\tan^2 \theta$  for  $\epsilon = 0.8$  (Thick solid),  $\epsilon = 0.4$  (thin solid), and  $\epsilon = 0.1$  (dotted curve).

magnetic fields  $\mathbf{B}_t \equiv \mathbf{B} - B_0 \mathbf{e}_y$  by introducing a parameter,  $\epsilon \equiv \int dV \mathbf{B}_t(t=0)^2 / \int dV B_0^2 = 0.1, 0.4, 0.8$ . We also carry out the simulation with  $\epsilon = 0.0$  to assess the validity of our simulation codes.

### 3. RESULTS

#### 3.1. Energy Exchange

Figure 1 shows the turbulent magnetic field energy density (color) and the magnetic field lines (white curves) at the initial state  $t\omega_{pe} = 0$  (left) and at the end of the simulation  $t\omega_{pe} = 1350$  (right) for  $\epsilon = 0.1$ . It is clearly shown that the turbulent magnetic field energy given at the initial state (bright spots in the left panel) decreases at the end of the simulations (right panel). The pattern size of the turbulent magnetic fields becomes relatively smaller with time. These results imply that the magnetic energy is converted to the plasma energy.

To see clearly how the energy conversion proceeds, we calculate deviations of each energy from the initial state, such as the electron kinetic energy  $\delta E_{\text{kin}} \equiv \sum_i m[\gamma(t) - \gamma(t=0)]/E_0$  and the turbulent magnetic field energies  $\delta E_{tB,xz} = \int dV \{(B_x^2 + B_z^2) - [B_x^2(t=0) + B_z^2(t=0)]\}/(8\pi E_0)$  and  $\delta E_{tB,y} = \int dV [B_y^2 - B_y^2(t=0)]/(8\pi E_0)$ , where  $E_0 = \int dV B_0^2/(8\pi)$  is the magnetic energy of uniform fields. Figure 2 depicts the time evolution of the energy deviation of the electrons  $\delta E_{\text{kin}}$  (solid curves) and of the minus of the turbulent magnetic energies  $-\delta E_{tB,xz}$  (dashed curves) and  $-\delta E_{tB,y}$  (dot-dashed curves). It can be seen that the turbulent magnetic energy in the perpendicular direction ( $\delta E_{tB,xz}$ ) decreases with time (note the minus sign), while the particle kinetic energy ( $\delta E_{\text{kin}}$ ) increases with it. The energy deviation of the particles  $\delta E_{\text{kin}}$  is almost comparable to  $-\delta E_{tB,xz}$ . This means that the perpendicular component of the magnetic energy is preferentially converted to the particle energy. Here it should be noted that the small difference between  $\delta E_{\text{kin}}$  and  $-\delta E_{tB,xz}$  comes from the electric field energy generated by turbulent motions. The particle energy distribution function obtained in this simulation can be well fitted by the Maxwellian distribution. Therefore, the plasma is not accelerated, but is heated up through the particle-wave interaction. The resulting heating is expected to become larger for models with larger initial turbulent magnetic energy (see models

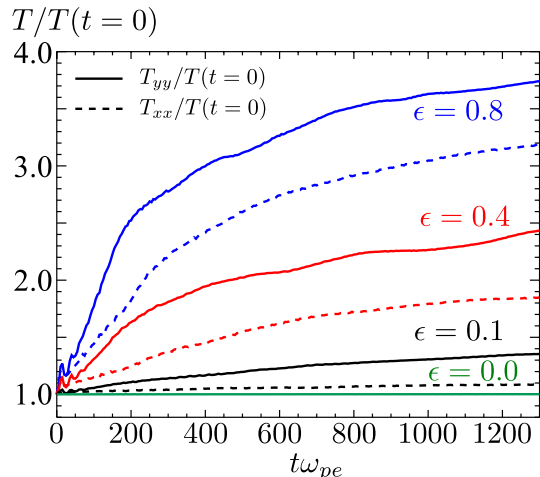


FIG. 5.— Time evolution of the electron temperature. Blue, red, black, and green curves are, respectively, for  $\epsilon = 0.8, 0.4, 0.1, 0.0$  and solid and dashed curves are for  $T_{yy}$  and  $T_{xx}$ , respectively.

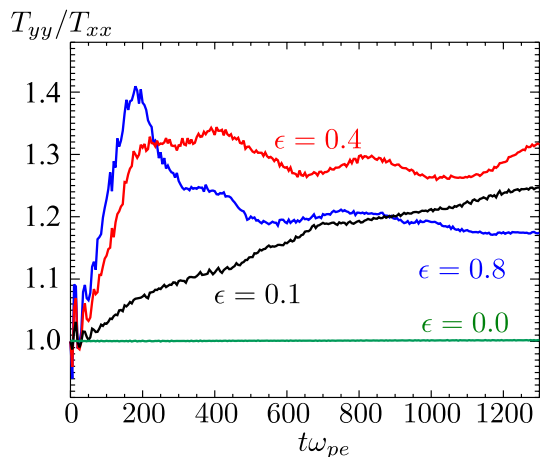


FIG. 6.— Time evolution of the ratio of the electron temperature  $T_{yy}/T_{xx}$ . Blue, red, black and green curves are  $\epsilon = 0.8, 0.4, 0.1, 0.0$ , respectively.

with different  $\epsilon$  in Figure 2). The efficient energy conversion to the perpendicular component also suggests that the energy dissipation will proceed anisotropically, which acts to make the configuration of the magnetic-field lines approach to the uniform one, i.e., the potential field.

#### 3.2. Anisotropy

To see the anisotropy more in detail, we perform the Fourier analysis of the magnetic fields. Top panels of Figure 3 show the power spectral density (PSD) of the turbulent magnetic field  $|\widehat{\mathbf{B}}_t/B_0|^2$  at  $t\omega_{pe} = 1350$ . It can be seen that the anisotropic turbulence preferentially transports the magnetic energy perpendicular to the uniform magnetic fields. The PSD is larger for a larger  $\epsilon$ , suggesting that the larger amplitudes of the turbulence lead to an efficient electron heating. The lower panels of Figure 3 show 1-dimensional cumulative power spectrum densities of the turbulent magnetic fields at  $t\omega_{pe} = 1350$ . The cumulative spectrum is defined as  $|\widehat{\mathbf{B}}_t(k_x)|^2 = \sum_{k_y} |\widehat{\mathbf{B}}_t(k_x, k_y)|^2$  (thick solid curves) and

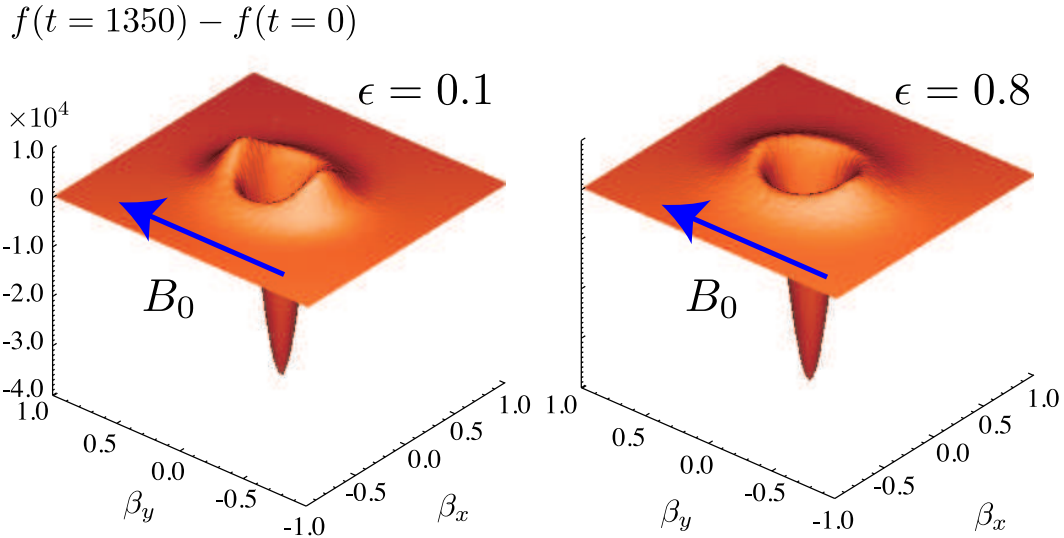


FIG. 7.— Deviation of the electron distribution function at  $t\omega_{pe} = 1350$  from the initial state at  $t\omega_{pe} = 0$  in  $\beta_x - \beta_y$  plane. Blue arrows denote the direction of the uniform magnetic fields  $\mathbf{B}_0$ . Left and right panels denote for  $\epsilon = 0.1$  and  $0.8$ , respectively.

$|\widehat{\mathbf{B}}_t(k_y)|^2 = \sum_{k_x} |\widehat{\mathbf{B}}_t(k_x, k_y)|^2$  (thin solid). The summation in  $k$ -space is performed in the range of  $0 < k_x, k_y < 10$  to reduce thermal noises. Dashed curves show the initial turbulent spectrum, which is isotropic in  $k_x$ - $k_y$  space. From these panels, the turbulent magnetic fields are shown to proceed via the forward cascade perpendicular to the uniform magnetic fields. The PSD in the perpendicular direction has a clear power-law distribution. Also the PSD in parallel direction also deviates from the initial (gaussian) distribution for a larger  $k$ . It suggests that the turbulent energy is mainly transported in perpendicular direction, but a some part of the energy (a few percent) is transported in the parallel direction.

To visualize the time evolution of the anisotropy, we show the time evolution of a quantity  $\theta$  in Figure 4,

$$\tan^2 \theta = \frac{\int dk_x dk_y k_x^2 |\widehat{\mathbf{B}}_t|^2}{\int dk_x dk_y k_y^2 |\widehat{\mathbf{B}}_t|^2}, \quad (8)$$

(see Shebalin et al. 1983; Saito et al. 2008). As already mentioned, the turbulent eddies interact each other with time more frequently for a larger  $\epsilon$ , transferring the turbulent energy to smaller scales. When  $t\omega_{pe} \lesssim 100$ , the anisotropic cascades proceed faster for a larger  $\epsilon$  because the cascade rate is an increasing function of the fluctuation. The turbulent energy is then transferred to the smaller scale. After that, the anisotropy  $\theta$  saturates almost at a constant level. The saturation level is shown to be highest for  $\epsilon = 0.4$  among the computed models. This is because too much initial turbulent energy (like  $\epsilon = 0.8$ ) disturbs the direction of the uniform magnetic fields, acting to smearing out the anisotropy.

### 3.3. Electron Heating

Now we are in a position to evaluate the temperature of electrons heated by the particle-wave interactions mentioned above. In doing so, we utilize the energy-momentum tensor as

$$T^{\mu\nu} = \frac{\int d^3\mathbf{p} f(\mathbf{p}) p^\mu p^\nu / e}{m_e \int d^3\mathbf{p} f(\mathbf{p})}, \quad (9)$$

where  $e$ ,  $p^\mu$  and  $f$  are the electron energy, the electron four momentum, and the electron distribution function, respectively. It should be noted that the temperature obtained from this equation is evaluated in the observer frame, while it should be naturally defined in the comoving frame. However this simplification is good enough in our case because the averaged velocity of electrons in mostly random motions is much smaller than the speed of light.

Figure 5 shows the time evolution of the electron temperature. It can be seen that the electron temperature parallel to the uniform magnetic field ( $T_{yy}$ , solid curves) increases with time faster than the perpendicular one ( $T_{xx}$ , dashed curves), and then  $T_{yy}$  becomes larger than  $T_{xx}$ . It is also shown that the electrons are heated more rapidly for a larger  $\epsilon$  because the turbulent energy cascade proceeds faster. Figure 6 shows the time evolution of the ratio of  $T_{yy}$  and  $T_{xx}$ . Before  $t\omega_{pe} < 200$ , the anisotropy of the electron temperature increases with time faster for a larger  $\epsilon$ . In this epoch, the electron is preferentially heated in the direction parallel to the uniform magnetic fields. Later on, the ratio approaches to a nearly constant value. The saturation level is highest for  $\epsilon = 0.4$  by the same reason as mentioned above (e.g., Figure 4).

Figure 7 shows the deviation of the electron distribution function at  $t\omega_{pe} = 1350$  from the initial state at  $t\omega_{pe} = 0$  for  $\epsilon = 0.1$  (left panel) and  $\epsilon = 0.8$  (right panel) on the plane of  $\beta_x - \beta_y$  with  $\beta_i \equiv v_i/c$  being the three velocity normalized by the speed of light. It can be seen that the distribution function is strongly distorted in the  $y$ -direction for  $\epsilon = 0.1$ . Considering the cascading process in perpendicular direction and the electron heating along the uniform magnetic fields, a Landau resonance ( $\omega = k_y v_y$ ) is the main mechanism for the electron heating. The electromagnetic waves generated by the turbulent motion can interact with electrons, which results in the Landau resonance.

Figure 8 shows the electron distribution function at  $t\omega_{pe} = 1350$  for  $\epsilon = 0.1$  (left) and for  $\epsilon = 0.8$  (right) on the plane of  $\beta_x - \beta_y$ . As mentioned above, the distri-

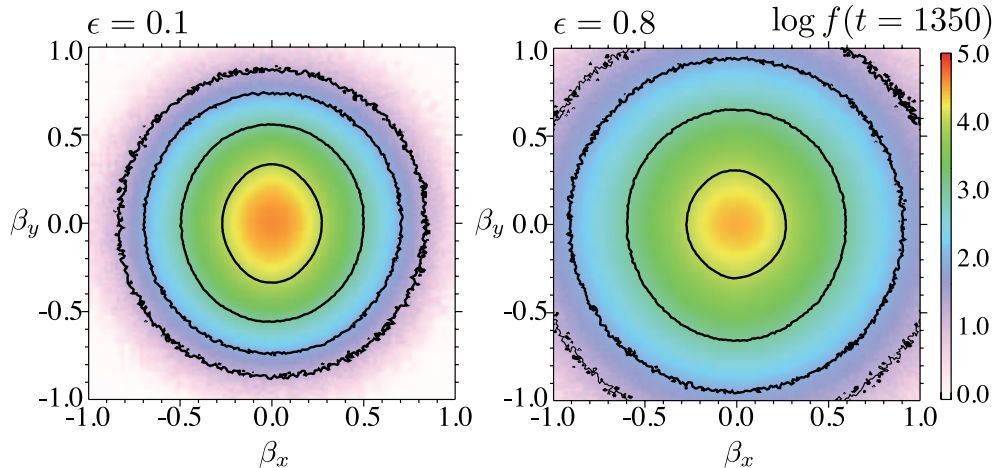


FIG. 8.— Electron distribution function at  $t\omega_{pe} = 1350$  for  $\epsilon = 0.1$  (left) and for  $\epsilon = 0.8$  (right) on the plane of  $\beta_x - \beta_y$ .

bution function is distorted in parallel direction because of the electron heating due to the Landau resonance. It should be noted that in both cases, the electrons with higher energies (i.e., a larger  $\beta$ ) are shown to get energies also in the direction perpendicular to the uniform magnetic fields, thus making the distribution function almost isotropic (see also Figure 2 that also shows the decrease in the parallel component of the magnetic field). This indicates that not only the Landau resonance, but also the cyclotron resonance ( $\omega = k_y v_y + \omega_{ce}$ ) plays a role of the electron heating and the dissipation of the turbulent magnetic energy (e.g., Saito et al. 2008). While the direction of the electron heating is parallel to  $B_0$  for the Landau resonance, there is an energy exchange between the waves and the perpendicular motion of the particles when the cyclotron resonance occurs (see, e.g., Gary 1993). It is also interesting to note that the energy dissipation rate of the cyclotron resonance obtained in this simulation is almost comparable to that of the Landau resonance, which has been known to be the case only in the linear regime (Miyamoto 2005). The dispersion relation of parallel propagating waves of  $E_x$  is shown in Figure 9 (color contour). The dashed curves denote the dispersion relations for the  $R$ -mode (top and bottom curves) and  $L$ -mode (middle curve) obtained from the linear analysis. Although the  $L$ -mode waves are generated by the turbulent motion, it is noted that they do not exchange energies with electrons since their polarization is in an opposite direction to the mean magnetic fields. The  $L$ -mode electromagnetic waves can interact mainly with ions but they are now assumed to be immovable as already mentioned. Thus the turbulence is maintained by the  $R$ -mode (whistler) waves in the electron scale.

Comparing to the results of the linear analysis (dashed lines), the dispersion relation obtained from the numerical results is not so clear, mainly because the large amplitudes of the turbulent magnetic fields injected at the initial state proceed forward cascades. By boldly extrapolating the agreement with the linear analysis with respect to the  $R$ -mode wave (whistler wave) for  $k_y c / \omega_{pe} \lesssim 1.0$  (bottom line), the  $R$ -mode wave in the higher  $k_y$  regime would be damped due to the cyclotron resonance. The findings of this paper (i.e., the occurrence of the heating both in the parallel and perpendicular direction as well

as the presence of the  $R$ -mode damping) suggest that the Landau resonance and the cyclotron resonance would be pivotal factors for the dissipation of the magnetic energy and the resulting electron heating.

#### 4. SUMMARY AND DISCUSSIONS

Bearing in mind the application to the outer crust of the NS, we investigated the turbulent magnetic field decay by means of the fully relativistic 2-dimensional PIC simulations. In the numerical simulations, the initial magnetic fields were set to be composed both of the uniform magnetic fields that model the global fields penetrating the NS and of the turbulent magnetic fields that would be originated from the Hall cascade of the large-scale turbulence. We showed that the turbulent whistler cascade transports the magnetic energy preferentially in the direction perpendicular to the uniform magnetic fields. It was also found that the distribution function of electrons becomes anisotropic because electrons with lower energies are predominantly heated in the direction parallel to the uniform magnetic fields due to the Landau resonance, while electrons with higher energies are heated mainly by the cyclotron resonance that makes the distribution function isotropic for the high energy tails. Furthermore we pointed out that the degree of anisotropy takes maximum as a function of the initial turbulent magnetic energy. This is because too much initial turbulent energy disturbs the direction of the uniform magnetic fields, acting to smearing out the anisotropy. The findings of this paper suggest that the particle-wave interactions via the Landau resonance and the cyclotron resonance, alternative to the conventional particle-particle collisions via the Ohmic dissipation, would be a pivotal dissipation mechanism in the outer crust of NSs.

The initial turbulent magnetic fields assumed in this study are relatively larger compared to the previous work (Saito et al. 2008; Gary et al. 2008). For  $\epsilon < 0.4$  in our simulation, the obtained results of the anisotropic cascade and the electron heating are basically consistent with the previous studies. As already mentioned, the anisotropy of the temperature decreases as  $\epsilon$  increases furthermore since the turbulent fields disturb the direction of the uniform magnetic fields. Although the tem-

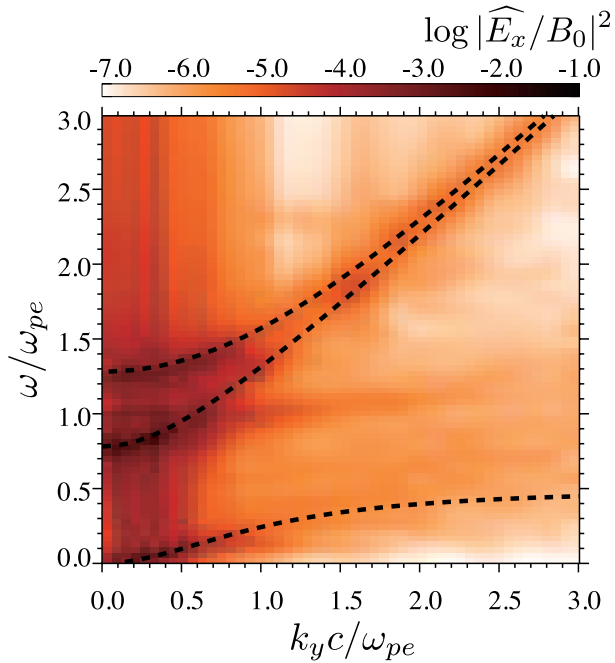


FIG. 9.— Dispersion relation of parallel propagating waves of  $E_x$ . The color shows the numerical result for  $\epsilon = 0.1$ . The dashed curves represent the dispersion relations for the  $R$ -mode (top and bottom) and  $L$ -mode (middle) obtained from the linear analysis.

perature becomes nearly isotropic, it should be noted that the cascading process itself is still anisotropic. According to Cho & Lazarian (2004, 2009), the small eddy (with size  $\sim l$ ) of the turbulent magnetic fields  $\mathbf{b}_l$  interacts not with the global magnetic fields  $B_0$ , but with the 'local' mean magnetic fields  $\mathbf{B}_L$ . Thus even when the turbulent magnetic field energy is much smaller than that of the uniform magnetic fields (especially  $B_0 = 0$ ), the cascading process should be locally anisotropic along  $\mathbf{B}_L$ . Such diffusion processes lead to the anisotropic heating of electrons, however the resulting electron temperature is in average isotropic, which should be the case obtained for high  $\epsilon$  in our simulation.

In the conventional model of the magnetic field decay, the magnetic fields are considered to be dissipated through the collisional process, namely via the Ohmic dissipation. While in this paper, we proposed that the magnetic fields are dissipated due to the Landau and cyclotron resonances, leading to the plasma heating in the collisionless regime. Since the wave-particle interactions occur in a very small scale ( $\sim$  gyro radius), the corresponding timescale ( $\sim \omega_{ce}^{-1}$ ) is much shorter than that

of the Ohmic dissipation, and it is instantaneous compared to the expected magnetic field decay timescale in the NSs. This means that the decay timescale should be determined by the cascading processes of the magnetic fields *above* the electron inertia scale. Although the PIC simulations have an advantage in its capability to determine the dissipation processes consistently, it is still computational too expensive to perform the PIC simulations covering over such a wide spacial range required to estimate the timescale. For the purpose, we think it important to perform the EMHD simulations including a phenomenological diffusivity which is adjusted to mimic the dissipation obtained in this study. Although this is apparently beyond the scope of this paper, we regard it as one of the most important tasks, which we plan to investigate as a sequel of this study.

So far there have been extensive work that focuses on the origin of the observed anisotropy in the NSs' surface temperature (e.g., Geppert et al. 2004; Pons & Geppert 2007; Aguilera et al. 2008; Pons et al. 2009). Unfortunately it is hard for us to do so immediately because the anisotropy obtained in the current simulation is confined in a very small scale (collisionless scale). To clarify how the particle-particle collisions in the more larger scales redistribute the electron distribution function and the resulting global temperature could be, one may need a new simulation technique which bridges the PIC simulation and the global (E)MHD simulations, albeit not an easy job at present. In addition to the NSs' surface, we speculate that the anisotropy due to the Landau resonance could be important also in the pulsar atmosphere because the plasma density is so small that the plasma there is expected to be globally collisionless. The consideration of the electron heating due to the Landau and cyclotron resonances might make the origin of the observed temperature anisotropy of NSs (Zavlin 2007; Haberl 2007; Nakagawa et al. 2009) less mysterious, which we are going to study one by one as an extension of this study.

Numerical computations were carried out on Cray XT4 at Center for Computational Astrophysics, CfCA, of National Astronomical Observatory of Japan and on Fujitsu FX-1 at JAXA Supercomputer System (JSS) of Japan Aerospace Exploration Agency (JAXA). This study was supported in part by the Grants-in-Aid for the Scientific Research from the Ministry of Education, Science and Culture of Japan (Nos. 19540309 and 20740150).

#### REFERENCES

- Aguilera, D. N., Pons, J. A., & Miralles, J. A. 2008, *A&A*, 486, 255
- Arras, P., Cumming, A., & Thompson, C. 2004, *ApJ*, 608, L49
- Bhattacharya, D., Wijers, R. A. M. J., Hartman, J. W., & Verbunt, F. 1992, *A&A*, 254, 198
- Bhattacharya, D., & Srinivasan, G. 1995, *X-ray Binaries*, 495
- Birdsall, C. K. & Langdon, A. B. 2001, *Plasma Physics via Computer Simulations* (New York, McGraw-Hill, 2001)
- Biskamp, D., Schwarz, E., Zeiler, A., Celani, A., & Drake, J. F. 1999, *Physics of Plasmas*, 6, 751
- Biskamp, D. & Welter, H. 1989, *Physics of Fluids B*, 1, 1964
- Cho, J. & Lazarian, A. 2004, *ApJ*, 615, L41
- . 2009, *ApJ*, 701, 236
- Cho, J., Lazarian, A., & Vishniac, E. T. 2002, *ApJ*, 566, L49
- Cordes, J. M., & Chernoff, D. F. 1998, *ApJ*, 505, 315
- Faucher-Giguère, C.-A., & Kaspi, V. M. 2006, *ApJ*, 643, 332
- Gary, S. P. 1993, *Theory of Space Plasma Microinstabilities*, ed. Gary, S. P.
- Gary, S. P., Saito, S., & Li, H. 2008, *Geophys. Res. Lett.*, 35, 2104
- Gary, S. P., Saito, S., & Narita, Y. 2010, *ApJ*, 716, 1332
- Geppert, U., Küker, M., & Page, D. 2004, *A&A*, 426, 267
- Goldreich, P. & Reisenegger, A. 1992, *ApJ*, 395, 250
- Goldreich, P. & Sridhar, S. 1995, *ApJ*, 438, 763
- Gonthier, P. L., Van Gilder, R., & Harding, A. K. 2004, *ApJ*, 604, 775
- Haberl, F. 2007, *Ap&SS*, 308, 181

- Harding, A. K., & Lai, D. 2006, Reports on Progress in Physics, 69, 2631
- Lyutikov, M., 2006, MNRAS, 367, 1594
- Miyamoto, K. 2005, Plasma Physics and Controlled Nuclear Fusion (Springer, ISBN 3540242171, 2005, 371 p.)
- Nakagawa, Y. E., Mihara, T., Yoshida, A., Yamaoka, K., Sugita, S., Murakami, T., Yonetoku, D., Suzuki, M., Nakajima, M., Tashiro, M. S., & Nakazawa, K. 2009, PASJ, 61, 387
- Narayan, R. & Ostriker, J. P. 1990, ApJ, 352, 222
- Narita, Y. & Gary, S. P. 2010, Annales Geophysicae, 28, 597
- Pons, J. A., & Geppert, U. 2007, A&A, 470, 303
- Pons, J. A., Link, B., Miralles, J. A., & Geppert, U. 2007, Physical Review Letters, 98, 071101
- Pons, J. A., Miralles, J. A., & Geppert, U. 2009, A&A, 496, 207
- Reisenegger, A. 2009, Revista Mexicana de Astronomia y Astrofisica Conference Series, 35, 139
- Saito, S., Gary, S. P., Li, H., & Narita, Y. 2008, Physics of Plasmas, 15, 102305
- Shebalin J. V., Matthaeus W. H., Montgomery D., 1983, Journal of Plasma Physics, 29, 525
- Shternin, P. S. & Yakovlev, D. G. 2006, Phys. Rev. D, 74, 043004
- Thompson, C., & Duncan, R. C. 1995, MNRAS, 275, 255
- Thompson, C., & Duncan, R. C. 1996, ApJ, 473, 322
- Woods, P. M., & Thompson, C. 2006, Compact stellar X-ray sources, 547
- Zavlin, V. E. 2007, arXiv:astro-ph/0702426